J Mater Sci (2008) 43:4175–4181
DOI 10.1007/s10853-008-2573-6

Particle size dependence of optical and defect parameters in mechanically milled Fe_2O_3

Mahuya Chakrabarti · A. Banerjee · D. Sanyal · Manas Sutradhar · Alok Chakrabarti

Received: 28 November 2007 / Accepted: 26 February 2008 / Published online: 26 April 2008

Abstract Fe_2O_3 of particle sizes ranging from 120 to 20 nm has been prepared by the ball-milling process using different milling hour. X-ray diffraction technique and transmission electron microscopy have been used for determining the average particle sizes of the prepared samples. Direct optical band gap for the unmilled and the ball-milled samples has been calculated from the optical absorption data. A red shift in the band gap due to the reduction of particle size has been observed. The coincidence Doppler broadening of the electron positron annihilation γ-radiation spectroscopy has been employed to identify the nature of defects generated due to the ball-milling process.

Introduction

Presently, oxides in its nanocrystalline phase become very important due to their wide applications. The large surface-to-volume ratio of these nanomaterials makes them different from the bulk of the material [1]. Among them, magnetic nanomaterials have received special attention as they can be used in different fields like magnetic resonance imaging, drug delivery agents, etc. [2]. Further, the observation of peculiar characteristics like superparamagnetism [3] in the nanoparticle phase of such materials makes these materials objects of great interest for fundamental studies. Among different magnetic nanoparticles, α-Fe_2O_3 has large applications in chemical industry [4]. It can be used as catalyst, gas sensing material to detect combustible gases [5] like CH_4 and C_3H_8 etc. α-Fe_2O_3, generally a rhombohedrally centered hexagonal structure [6], is the most stable polymorph in nature under ambient condition and can be easily found in mineral hematite.

Nanocrystalline oxides can be prepared by different methods, e.g., sol–gel [7], hydrothermal [8], chemical vapor phase deposition [9], calcinations of hydroxides [10], radio frequency sputtering [11], gas condensation technique [12], high-energy ball-milling process [13, 14], etc. Among these the high-energy ball-milling process has many potential advantages. The main advantage is large quantities of samples can be produced in a very short time, and the process is relatively simple and inexpensive.

In the present work, ball-milling process has been adapted to prepare nanocrystalline Fe_2O_3 samples. The optical and defect properties of the prepared nanocrystalline samples have been studied by employing UV spectroscopy and coincidence Doppler broadening of the electron positron annihilation γ-radiation (CDBEPAR) spectroscopy, respectively. Employing the UV absorption spectroscopic method [15] the changes in the band gap for direct transitions for all the samples (milled and unmilled Fe_2O_3) have been measured. The defect parameter in the band gap has also been estimated from the optical absorption data.

During the preparation of nanocrystalline oxides by the ball-milling process, large numbers of defects are introduced in the material [14–16]. In the nanocrystalline phase the surface-to-volume ratio is very high, hence the surface

M. Chakrabarti (✉) · D. Sanyal · A. Chakrabarti
Variable Energy Cyclotron Centre, 1/AF, Bidhannagar, Kolkata 700064, India
e-mail: mahuya@veccal.ernet.in

A. Banerjee
Department of Physics, University of Burdwan, Golapbag, Burdwan 713104, India

M. Sutradhar
Department of Chemistry, University of Calcutta, 92, Acharya Prafulla Chandra Road, Kolkata 700009, India

defects play important role in determining the optical, magnetic, and electronic properties of the material. Thus it is very important to study these defects. Presently, CDBEPAR spectroscopic technique, a powerful technique to study the defects in a material [17, 18], has been employed to study the defects in the different hour ball milled as well as the unmilled samples.

In the CDBEPAR spectroscopic technique, positron from the radioactive (^{22}Na) source is thermalized inside the material under study and annihilate with an electron emitting two oppositely directed 511 keV γ-rays. Depending upon the momentum of the electron (p) these 511 keV γ-rays are Doppler shifted by an amount $\pm\Delta E$ in the laboratory frame, where $\Delta E = p_L c/2$; p_L being the component of the electron momentum p toward the detector direction. By using two identical high-resolution HPGe detectors one can measure the Doppler shifts of these 511 keV γ-rays [18]. The wing part of the 511 keV photo peak carries the information about the annihilation of positrons with the higher momentum electrons, e.g., core electrons of different atoms. Thus by measuring the Doppler broadening of the 511 keV γ-ray and proper analysis of the CDBEPAR spectrum [14] one can identify the electrons with which positrons are annihilating.

Experimental outline

α-Fe_2O_3 of purity 99.998% (Alfa Aesar, Johnson Matthey, Germany) has been milled in a Fritsch Pulverisette 5 planetary ball mill grinder with agate balls for different hours to achieve lower particle size. The ball-to-powder mass ratio has been fixed to 12:1. The powder X-ray diffraction (XRD) data has been collected in a Philips PW 1710 automatic diffractometer with CuK_α radiation. In each case scanning has been performed in between the 2θ range 20–90° in a step size of 0.02°. The average particle size of the sample has been calculated from Williamson–Hall plot [19]

$$\beta\cos\theta = K\lambda/D + 2\varepsilon\sin\theta$$

where D is the average particle size, β is the full width at half maximum (FWHM), K is a constant (=0.89), λ is the wavelength; θ is the Bragg angle, and ε is the strain introduced inside the sample. The XRD patterns (Fig. 1) for differently milled and unmilled samples show α-Fe_2O_3 lines only, implying that none of the other oxide phases have been developed during ball milling.

Transmission electron microscopy (TEM) with TECNAI S-TWIN (FEI Company) electron microscope operating at 200 kV has been used to estimate the average particle size of the different hour ball-milled Fe_2O_3 samples. Powder ultrasonically dispersed in alcohol was put on a standard microscope grid for the TEM work.

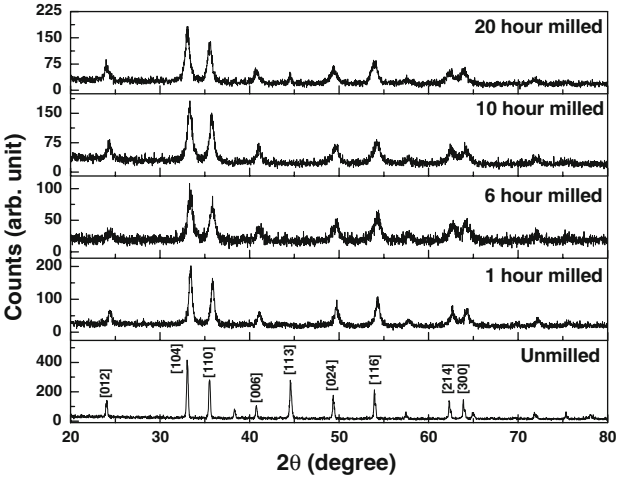

Fig. 1 X-ray diffraction pattern for the unmilled and milled samples

For the CDBEPAR measurement, two identical HPGe detectors (*Efficiency*: 12%; *Type*: PGC 1216sp of DSG, Germany) having energy resolution of 1.1 keV at 514 keV of ^{85}Sr have been used as two 511 keV γ-ray detectors, while the CDBEPAR spectra have been recorded in a dual ADC-based multiparameter data acquisition system (MPA-3 of FAST ComTec., Germany). A 10 μCi ^{22}Na positron source (enclosed in between thin Mylar foils) has been sandwiched between two identical and plane faced pellets [20]. The peak-to-background ratio of this CDBEPAR measurement system, with $\pm\ \Delta E$ selection, is $\sim 10^5$:1 [21, 22]. The CDBEPAR spectrum has been analyzed by evaluating the so-called lineshape parameters [17, 21] (S parameter). The S parameter is calculated as the ratio of the counts in the central area of the 511 keV photo peak $\left(\left|511\,\text{keV} - E_\gamma\right| \le 0.85\,\text{keV}\right)$ and the total area of the photo peak $\left(\left|511\,\text{keV} - E_\gamma\right| \le 4.25\,\text{keV}\right)$. The S parameter represents the fraction of positron annihilating with the lower momentum electrons with respect to the total electrons annihilated. The statistical error is $\sim$0.2% on the measured lineshape parameters. The coincidence DBEPAR spectra for the unmilled and the milled samples have been also analyzed by constructing the "ratio-curves" [18, 21, 22] with respect to defects-free 99.9999% pure Al single crystal (reference sample). The electronic absorption spectra [23] of the Fe_2O_3 nanoparticles have been recorded on HitachiU-3501 spectrophotometer in the wavelength range of 200–1,500 nm.

Results and discussion

Figure 1 represents the XRD pattern for the unmilled, 1, 6, 10, and 20 h milled samples. Particle size as calculated from the Williamson–Hall plot for the unmilled sample is 120 nm. Figure 2 shows the Williamson–Hall plot for 2 h

milled sample. Particle size and the strain introduced inside the samples due to ball milling have been calculated from the intercepts and slope of the straight line fitted curve as shown in Fig. 2. Table 1 represents the particle sizes and strain values for the unmilled and the milled samples (calculated from the Williamson–Hall plot). From Table 1 it is clear that the strain increases with increasing milling hour. Increase of strain with the milling hour suggests the formation of defects in the milled sample.

Figure 3 shows the variation of particle size with milling hour. From Fig. 3 it is clear that with the ball-milling process the particle size cannot be lowered continuously, rather it becomes saturated after some specific milling hour.

Figure 4a–c represents the TEM micrographs for the unmilled, 10 and 20 h milled samples, respectively. From the TEM pictures the measured particle sizes are 206, 14, and 10 nm for unmilled, 10 h milled, and 30 h milled

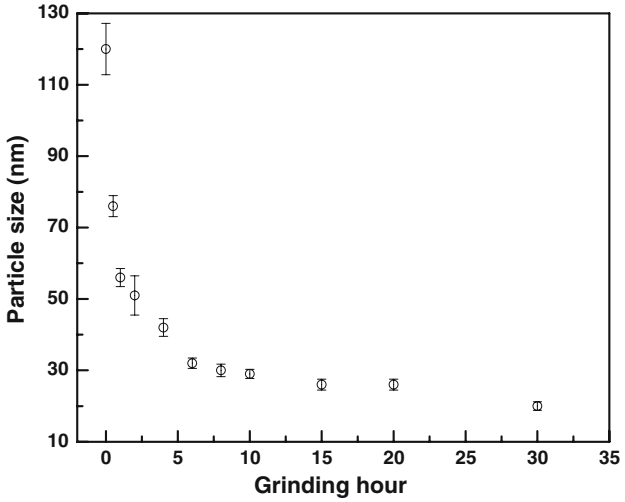

Fig. 3 Variation of particle size (estimaetd from Scherrer formula and Williamson–Hall plot) with milling hour

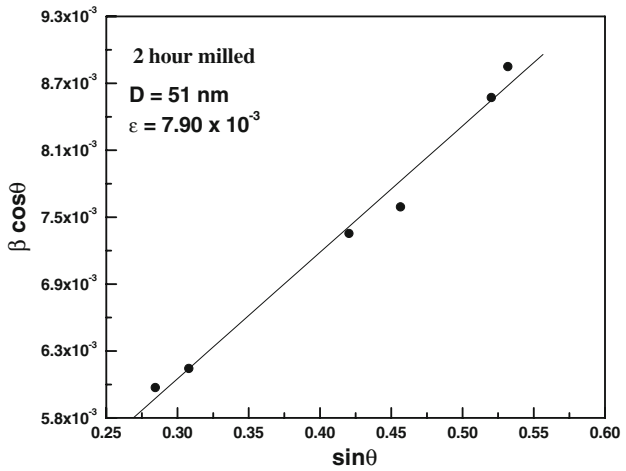

Fig. 2 Willamson–Hall plot for 1 h milled sample

Table 1 Value of strain for the unmilled and different hour ball milled samples

Milling hour	Particle size (nm)	Strain (%)
Unmilled	120	1.2×10^{-3}
30 min	76	2.0×10^{-3}
1 h	56	5.7×10^{-3}
2 h	51	7.9×10^{-3}
4 h	42	15.0×10^{-3}
6 h	32	11.6×10^{-3}
8 h	30	60.5×10^{-3}
10 h	29	84.2×10^{-3}
15 h	26	86.2×10^{-3}
20 h	26	86.5×10^{-3}
30 h	20	89.4×10^{-3}

samples, respectively. The lattice parameters "a" and "c" for the unmilled and milled samples have been calculated from different diffraction lines of the XRD pattern (Fig. 1). Figure 5 shows the variation of the lattice parameters "a" and "c" with milling hour. From Fig. 5 it is observed that both the lattice parameters ("a" and "c") decrease with increasing milling hour. This clearly indicates that with milling, large number of defects have been introduced inside the milled samples.

To observe the effect of milling in the band gap, the optical absorption spectroscopic technique has been used. The spectral absorption coefficient, α, is defined as [24]

$$\alpha(\lambda) = 4\pi k(\lambda)/\lambda$$

where $k(\lambda)$ is the spectral extinction coefficient obtained from the absorption curve and λ is the wavelength. Figure 6 represents the absorbance curve for unmilled, 8 h milled, and 20 h milled samples. The inset of Fig. 6 shows the absorbance curve in some specific wavelength region. From Fig. 6 it has been observed that in case of ball-milled (8 and 20 h) samples the absorption maxima occur at 303 and 306 nm, whereas for the unmilled sample the absorption maximum is at 304 nm. Thus the position of the absorption maxima remains almost the same for the unmilled and the 8 h milled samples, whereas for the 20 h milled sample it is on the longer wavelength side (306 nm).

The band gap, E_g (for a direct transition between the valence and conduction band), is obtained by fitting the experimental absorption data with the following equation

$$\alpha h\gamma \sim A(h\gamma - E_g)^{1/2} \text{ for a direct transition, [25]}$$

where $h\gamma$ is the photon energy, α is the absorption coefficient, E_g is the band gap, and A is a characteristic

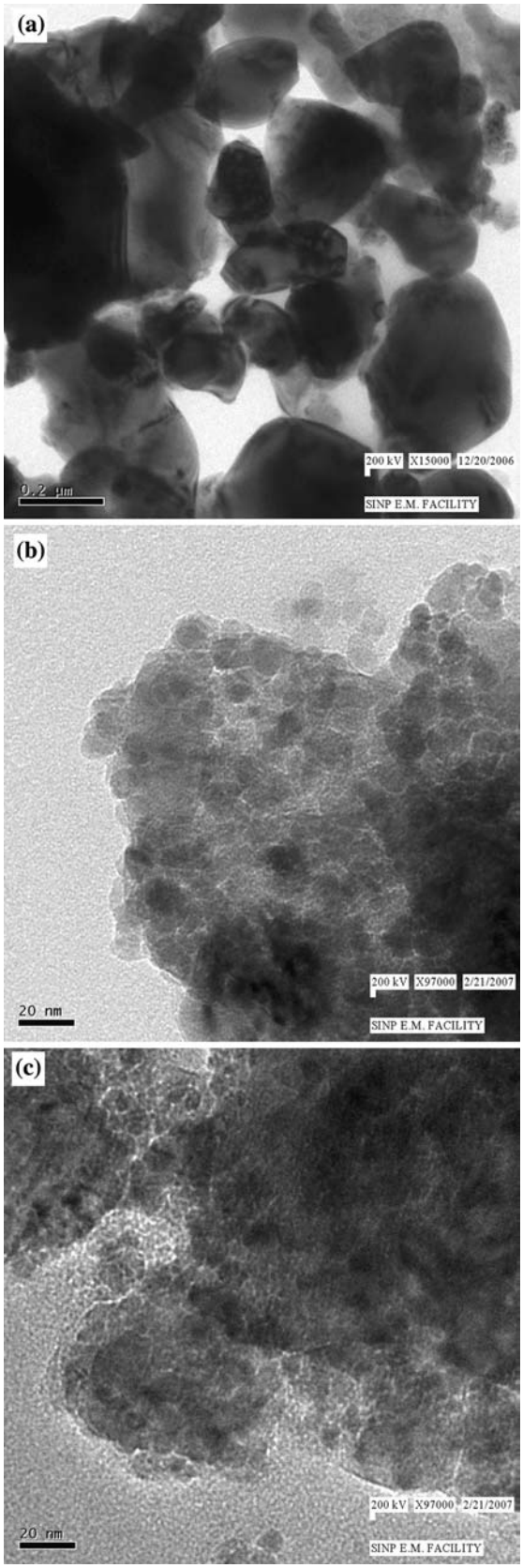

Fig. 4 TEM micrographs for (**a**) unmilled, (**b**) 10 h milled, and (**c**) 30 h milled Fe_2O_3 samples, respectively

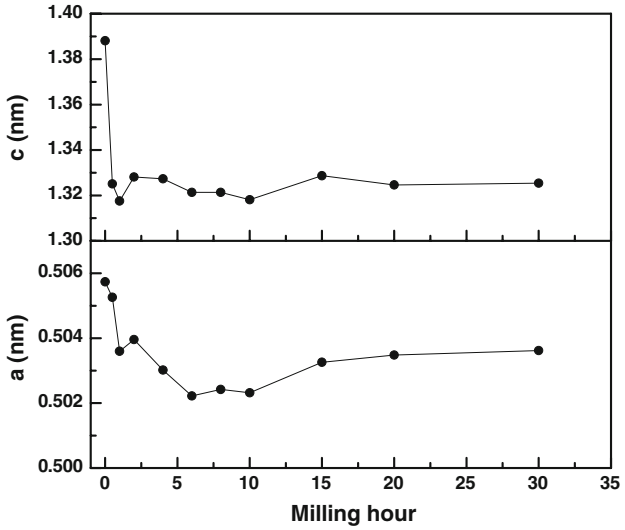

Fig. 5 Variation of lattice parameters ("*a*" and "*c*") with milling hour

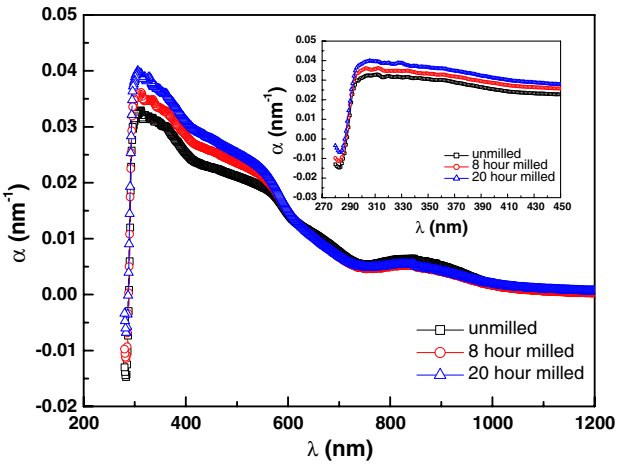

Fig. 6 Absorbance curve for unmilled, 8 h, and 20 h milled samples

parameter independent of photon energy. Figure 7a, b represent the absorption curves of different ball-milled Fe_2O_3 powder for direct transition. The value of band gap E_g (for direct transition) has been obtained from the intercept of the extrapolated linear part of the $(\alpha h\nu)^2$ versus $h\nu$ curve with the energy ($h\nu$) axis. The band gap for direct transition (estimated from Fig. 7a, b) for the unmilled sample is 2.62 eV at the wavelength 473 nm, whereas for 1, 4, 6, 8, 10, and 20 h milled samples it is 2.59, 2.56, 2.54, 2.52, 2.49, and 2.49 eV at 479, 485, 489, 493, 497, and 498 nm, respectively. The variation of the band gap (for direct transition) with the inverse of particle size (D) follows a linear fit with a negative slope (Fig. 8). The decrease of band gap with decreasing particle size may be due to the enhanced band bending effect [26, 27] at the

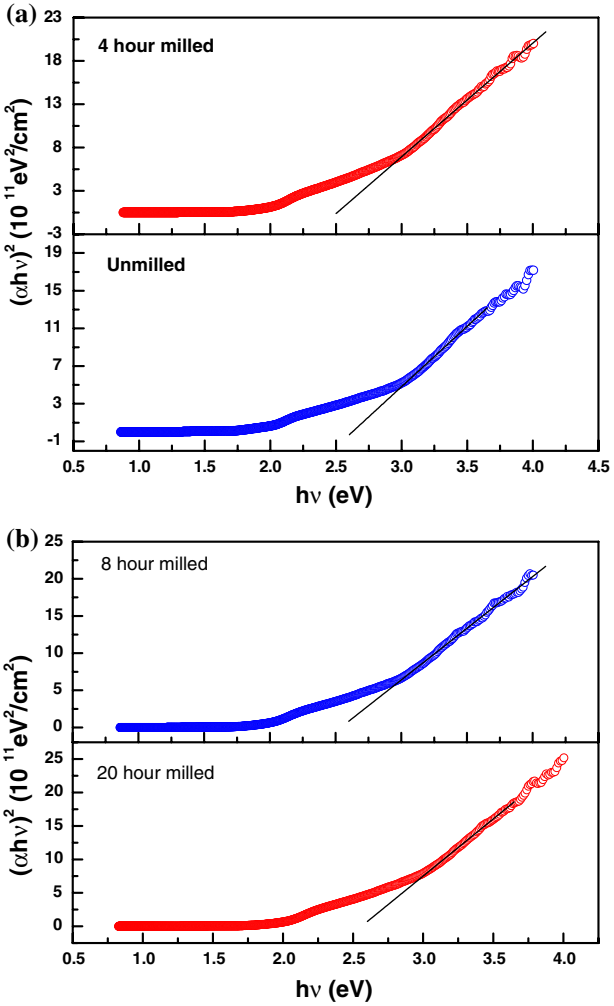

Fig. 7 (**a**) Absorption spectra for unmilled and 4 h milled samples for direct transition. (**b**) Absorption spectra for 8 and 20 h milled samples for direct transition

particle boundaries or may be due to the defects introduced in the milled samples.

In the energy region $h\nu < E_g$, i.e. near the band edge, the absorption coefficient follow the relation [23]

$$\alpha = \alpha_0 \exp(h\nu/E_0)$$

where α_0 is a constant and E_0 is an empirical parameter which represents the width of the band tail states. E_0 may be considered as the defect parameter in the band gap energy value [26]. E_0 can be obtained from the slope of the linear part of ln(α) versus E curve in the $E < E_g$ region. Figure 9 shows the ln(α) versus E curve for the unmilled, 8 h, and 20 h milled samples. The values of E_0 as calculated from the intercept of the extrapolated linear part of the ln(α) versus hν curve with the energy (hν) axis are plotted in Fig. 10 with inverse of the particle size (D). It is clear from Fig. 10 that with lowering the particle size (by increasing milling hour) the defect parameter E_0 increases

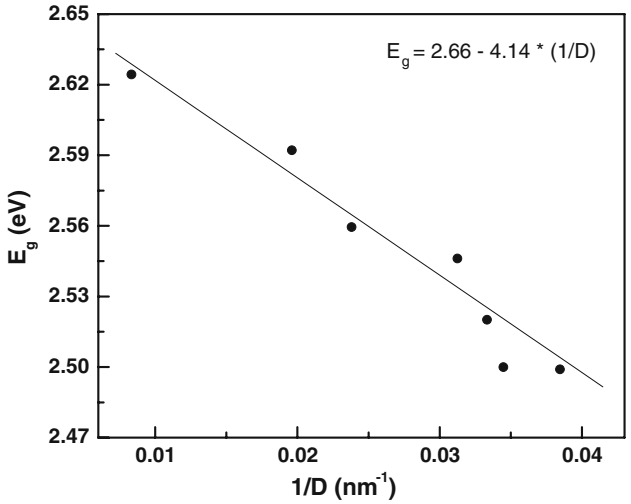

Fig. 8 Variation of band gap (E_g) with the inverse of particle size ($1/D$)

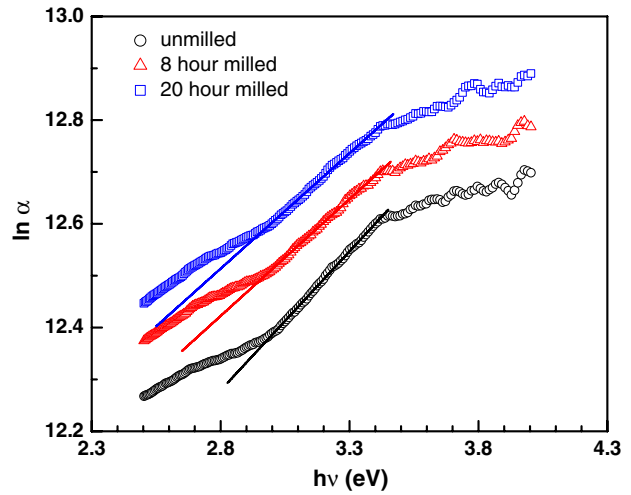

Fig. 9 Plots of ln(α) versus photon energy (E) for unmilled, 8 h, and 20 h milled samples

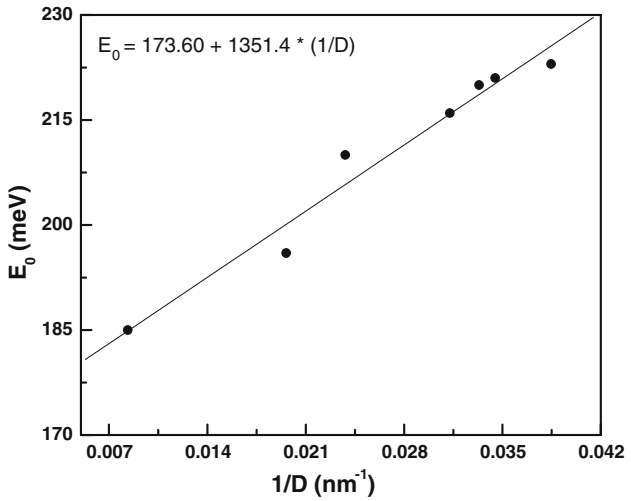

Fig. 10 Variation of E_0 with the inverse of particle size ($1/D$)

linearly. This confirms that lowering the particle size by increasing milling hour, a large number of defects have been introduced inside the samples.

To identify the defects, CDBEPAR measurement technique has been employed. In case of nanocrystalline materials, the positron diffusion length plays an important role, as after entering a material the positron becomes thermalized and diffuses inside the material. The typical positron diffusion length is ~100 nm [28], which is larger than the average particle size of the milled samples. Therefore, compared to the unmilled sample (particle size ~120 nm), positrons annihilate more at the grain surfaces in the milled samples.

Figure 11 represents the variation of *S* parameter with milling hour, where *S* parameter increases with milling hour. In general, the increase of the *S* parameter suggests either the positrons are less annihilating with the core electrons or an increase of the number of lower momentum electrons at the positron annihilation site [17, 20–22]. Thus from the variation of *S* parameter with milling hour it can be concluded that either positrons are less annihilating with the core electrons of Fe and O or more annihilating with the lower momentum electrons.

To identify the nature of defects in the milled samples, the CDBEPAR spectra for the unmilled and ball milled Fe_2O_3 have been analyzed by constructing the ratio curve [20, 29] with the CDBEPAR spectrum of the defect-free 99.9999% pure Al single crystal (Fig. 12). From Fig. 12 it is clear that there is a peak at $\sim 10 \times 10^{-3}\ m_0c$ and a flat region at $\sim 20 \times 10^{-3}\ m_0c$ for unmilled, 1 h, and 20 h milled samples. Using the relation $E = p^2/4m_0$ the kinetic energies of the electrons corresponding to momentum $p_L \sim 10 \times 10^{-3}\ m_0c$ and $20 \times 10^{-3}\ m_0c$ comes out to be ~13 and 51 eV, respectively. The annihilation of positrons with 2p core electrons of oxygen and 3d core electrons of Fe are mainly contributing to the peak at $10 \times 10^{-3}\ m_0c$, while the annihilation of positrons with the 3p core electrons of Fe contribute to the flat region ($p_L \sim 20 \times 10^{-3}\ m_0c$). Figure 13 represents the ratio curve for the ball-milled Fe_2O_3 with respect to unmilled Fe_2O_3. A broad dip from the momentum range $\sim 7 \times 10^{-3}\ m_0c$ to $\sim 22 \times 10^{-3}\ m_0c$ is prominent (Fig. 13) in the 20 h milled sample. Thus from Figs. 12 and 13 it can be concluded that positrons annihilation with the core electrons (both 3d and 3p) of Fe decreases with increasing milling hour. This indicates the formation of cation type of defects (Fe vacancy) at the grain

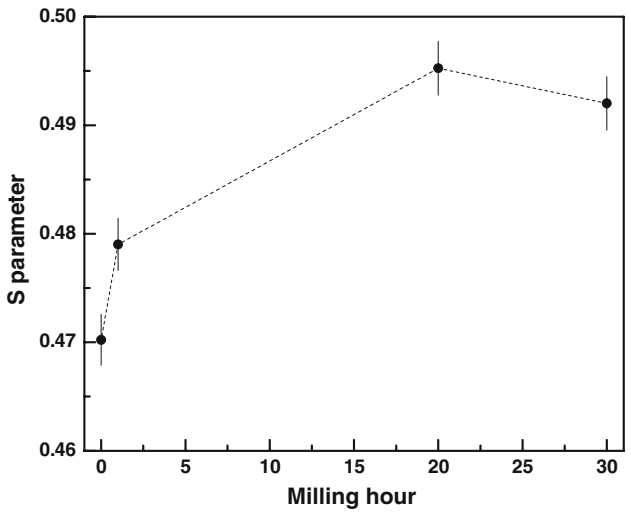

Fig. 11 Variation of *S* parameter with milling hour

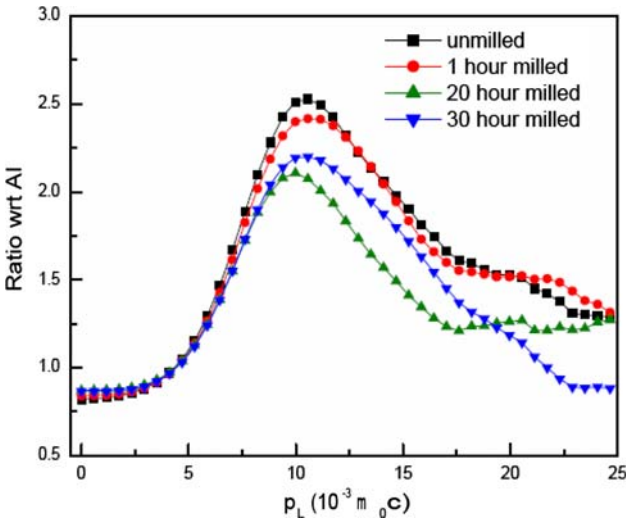

Fig. 12 Ratio of the experimental electron positron momentum distributions for unmilled, 1, 20, and 30 h milled Fe_2O_3 samples to the electron positron momentum distributions for the defect-free 99.9999% pure Al single crystal

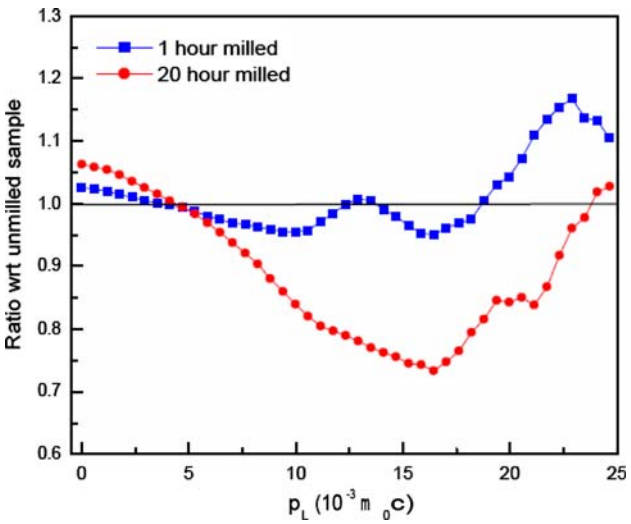

Fig. 13 Ratio of the experimental electron positron momentum distributions for 1 and 20 h milled Fe_2O_3 samples to the electron positron momentum distributions for the unmilled Fe_2O_3 samples

surface of the milled Fe_2O_3 system, which is in agreement with the earlier observation of formation of cation type of defects in different oxide samples due to the ball-milling process [14, 15].

Conclusions

Nanocrystalline Fe_2O_3 samples have been prepared by the ball-milling process. Particle sizes of the milled and the unmilled samples have been estimated from XRD pattern and TEM micrographs. The strain introduced inside the sample increases with ball milling hour. Ratio curve analysis of the CDBEPAR spectra for the different hour milled and unmilled samples indicates the formation of cation type of defects at the grain surfaces due to the ball-milling process. Direct optical band gap decreases with decreasing particle size but the defect parameter (as calculated from the band tail near the absorption edge of the absorption spectra) increases linearly with milling hour (or decreasing particle size). Finally, it has been concluded that due to ball milling the average particle size of the Fe_2O_3 decreases, but due to the formation of cation type of defects the optical band gap decreases.

Acknowledgements M. Chakrabarti and M. Sutradhar gratefully acknowledge CSIR, Government of India, for providing financial assistance. A. Banerjee gratefully acknowledges Prof. S. K. Pradhan, Department of Physics, Burdwan University, for his valuable suggestions. The authors are thankful to Prof. G. N. Mukherjee, Department of Chemistry, University of Calcutta, for the optical measurement. The authors are also thankful to Mr. P. Ray, SINP, Kolkata, for the TEM measurement and A. Kar Mahapatra, SINP, Kolkata, for the XRD measurement.

References

1. Henglin A (1989) Chem Rev 89:1861
2. Hinds KA et al (2003) Blood 102:867; Rudge SR, Kurtz TL, Vessely CR, Catterall LG, Williamson DL (2000) Biomaterials 21:1411
3. Jones DH (1989) Hyperfine Interact 47:289
4. Mimura N, Takahara I, Saito M, Hattori T, Ohkuma K, Ando M (1998) Catal Today 45:61
5. Huo L, Li W, Lu L, Cui H, Xi S, Wang J, Zhao B, Shen Y, Lu Z (2000) Chem Mater 12:790
6. Zboril R, Mashlan M, Petridis D (2002) Chem Mater 14:969
7. Pascual R, Sayer M, Kumar CVRV, Zou L (1991) J Appl Phys 70:2348
8. Wang X, Chen X, Ma XC, Zheng H, Ji M, Zhang Z (2004) Chem Phys Lett 384:391
9. Kim ET, Yoon SG (1993) Thin Solid Films 227:7
10. Bokhimi X, Morales A, Portilla M, Gracia-Ruiz A (1999) Thin Solid Films 12:589
11. Luo WG, Ding AL, Li H (1995) Integr Ferroelectr 9:75
12. Birringer R, Gleiter H, Klein HP, Marquardt P (1984) Phys Lett A 102:365
13. Michel D, Gaffet E, Berther P (1995) Nanostruct Mater 6:667
14. Chakrabarti M, Bhowmick D, Sarkar A, Chattopadhyay S, Dechoudhury S, Sanyal D, Chakrabarti A (2005) J Mater Sci 40:5265. doi:10.1007/s10853-005-0743-3
15. Chakrabartii M, Dutta S, Chattopadhyay S, Sarkar A, Sanyal D, Chakrabarti A (2004) Nanotechnology 15:1792
16. Zhang BQ, Lu L, Lai MO (2003) Physica B 325:120
17. Hautojarvi P, Corbel C (1995) In: Dupasquier A, Mills AP Jr (eds) Positron spectroscopy of solids. IOS Press, Amsterdam, p 491; In: Krause-Rehberg R, Leipner HS (eds) Positron annihilation in semiconductors, Springer Verlag, Berlin, 1999
18. Lynn KG, Goland AN (1976) Solid State Commun 18:1549
19. Williamson GK, Hall WH (1953) Acta Metall 1:22
20. Chakrabarti M, Sarkar A, Chattopadhyay S, Sanyal D (2006) In: Martins BP (ed) New topics in superconductivity research. Nova Science, New York
21. Chakrabarti M, Sanyal D, Chakrabarti A (2007) J Phys Condens Matter 19:236210
22. Sanyal D, Chakrabarti M, Roy TK, Chakrabarti A (2007) Phys Lett A 371:482
23. Pancove J (1979) Optical processes in semiconductors. Prentice-Hall, Englewood Cliffs, NJ
24. Dakhel AA, Henari FZ (2003) Cryst Res Technol 38:979
25. Tauc J (1970) Mater Sci Bull 5:72
26. Dutta S, Chattopadhyay S, Sutradhar M, Sarkar A, Chakrabarti M, Sanyal D, Jana D (2007) J Phys Condens Matter 19:236218
27. Srikant V, Clarke DR (1997) J Appl Phys 81:6357
28. Puska MJ, Nieminen RM (1994) Rev Mod Phys 66:841
29. Myler U, Simpson PJ (1997) Phys Rev B 56:14303